A Stable Loss Control Feedback Loop for VCO Amplitude Tuning

Faramarz Bahmani, *Member, IEEE*, and Edgar Sánchez-Sinencio, *Fellow, IEEE*

Abstract—In practical implementations of *LC* oscillators in which the quality factor of the tank is dominated by the quality factor of the inductor, due to dependence of the oscillation amplitude on the square of the oscillation frequency and the bias current of the *LC* tank, a stable amplitude control loop is essential to maintain a constant oscillation amplitude over the tuning range of the voltage-controlled oscillator (VCO) and to optimally bias the VCO over different conditions. In this paper, an enhanced loss control scheme incorporating an integral feedback to automatically tune the oscillation amplitude of *LC* oscillators is proposed. The proposed loss control feedback (LCF) loop is conditionally stable with an easy stability requirement to meet and its stability is examined: 1) by linearizing the system around the stable point using a perturbation method; and 2) by numerically solving the nonlinear differential equation of the LCF loop describing the transient behavior of the step response of the loop. A prototype including the *LC* VCO and the proposed LCF loop has been implemented in TSMC 0.35-μm CMOS process and occupies an area of 0.057 mm^2 and consumes 8.1 mA from a 2.8-V power supply. The LCF loop, with respect to the VCO, has an overhead of 25% on the area and consumes only 1.3% of the total power. Measurement results of the proposed LCF loop show an 11 dBm amplitude tuning range from -16 dBm to -5 dBm at any frequency over the 2–2.5-GHz tuning range of the VCO. The step response of the loop has a settling time less than 0.5 ns.

Index Terms—Automatic amplitude tuning, *LC* resonator, loss control, phase noise, Q-enhancement , stability, Van der Pol equation, voltage-controlled oscillator (VCO).

I. INTRODUCTION

WITH the constant shrinking of feature sizes and increasing clock speeds in integrated circuit (IC) technology, designers are approaching a widespread use of digital systems with clock speeds in the gigahertz range. One of the major challenges in the distribution and synchronization of these gigahertz clocks is on-chip phase-locked loop (PLL) clock multipliers which rely on the oscillation amplitude of *LC* voltage-controlled oscillator (VCOs) [1]. Since the oscillation amplitude of current-biased *LC* VCOs varies over its tuning range [2], an amplitude control scheme is needed to set the amplitude to a predefined level so the operation of the frequency dividers in the PLL is not compromised [3], [4].
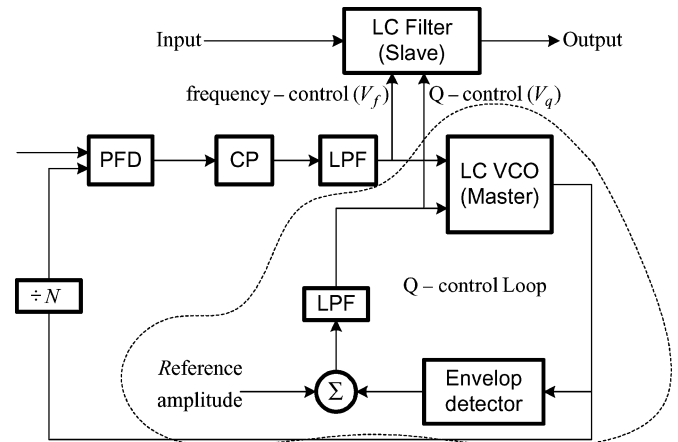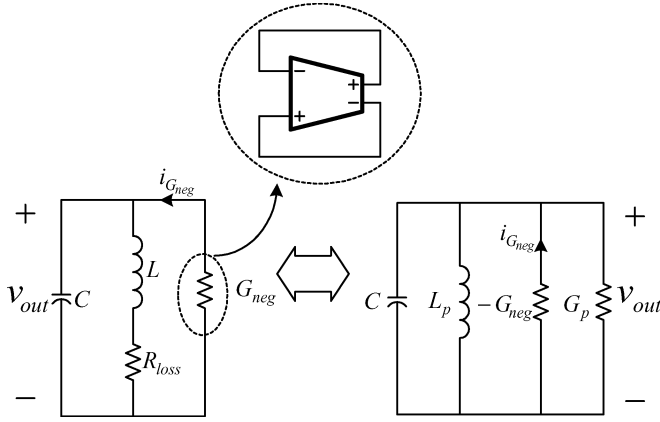
Fig. 1. Automatic tuning control method using PLL [7].

On the other hand, to ensure a clock with very low jitter, a high-quality *LC* tank is needed. However, the quality factor (Q_0) of practical on-chip inductors is typically very low ($\sim$3–5) and frequency dependent. The low quality factor and frequency dependence is mainly due to a lossy silicon substrate and thin metal layers. A great deal of attention has been focused on improving the performance of lossy *LC* tanks by introducing a negative transconductance to compensate its resistive loss [5]. By tuning this loss, and thus the Q factor of the *LC* tank, it is possible to control the amplitude of oscillation in an *LC* VCO implementation. The tuning results in a fast and reliable start up with an optimal bias point in terms of phase noise performance [6]. However, the bias current required by the oscillator depends on the amplitude of oscillation, the losses in the tank, and also other process and environment parameters. Consequently, if the VCO circuit is biased with a fixed current, oscillations over all conditions may not be guaranteed, nor can an optimum value to minimize power and ensure fixed amplitude of oscillation be found [4], [6].

Therefore, having a stable, efficient, and cost-effective mechanism to control the resistive loss of the *LC* tank can also be used to tune the quality factor of on-chip *LC* filters [7]. This concept is illustrated in Fig. 1. The PLL circuit locks the oscillation frequency of the VCO and thus the center frequency of the slaved filter. Assuming identical tanks for both VCO and filter, the Q control loop locks the oscillation amplitude to a reference signal, and feeds the same Q control voltage to the slaved resonator. In other words, the same concept used to tune the quality factor of the *LC* filters has been modified to regulate the oscillation amplitude. However, the main problem of using a VCO is its amplitude regulation during the tuning process. The oscillation amplitude should be large enough so that its zero-crossing points can

Fig. 2. Q-enhancement LC resonator.

Fig. 3. Oscillator with amplitude control feedback.

be detected by the loop and at the same time it should be small enough so that the negative resistor in the VCO can maintain its linear region of operation. Harmonic distortion and nonlinearities of the negative resistor can cause not only loss-control error, but also frequency-tuning error [12].

In this paper, a stable enhanced loss control feedback (LCF) loop is presented to automatically regulate, arbitrarily, the oscillation amplitude of an LC VCO. The VCO can achieve robust amplitude regulation while a significant frequency tuning range of 0.5 GHz around a 2.25-GHz frequency can be obtained.

In Section II, the principle of the Q-Enhanced LC resonator and its amplitude stability are discussed. The fundamentals of the currently available LCF techniques used to regulate the oscillation amplitude are also discussed in this section. The proposed LCF architecture and its stability properties are presented in Section III. Section IV presents the experimental results of a CMOS 0.35-μm test chip. Concluding remarks are given in Section V.

II. LCF MECHANISM

A. Amplitude Stability of LC Resonators

A lossless LC resonant tank has an ideal quality factor of infinity and, with a nonzero initial condition, produces a steady sinusoidal oscillation. However, mainly due to losses associated with the integrated spiral inductors, the achievable quality factor of the tank in the gigahertz frequency range is, in practice, low. This loss inhibits the oscillation. To over compensate the total loss of the LC tank, a Q-enhancement technique can be achieved by introducing a negative loss (resistor) through a positive feedback around the tank. Fig. 2 shows the conceptual implementation of the Q-enhancement technique [7], [8]. In the vicinity of the resonant frequency ω_0, the series combination of the inductor L and its resistive loss R_{loss} can be modeled as a parallel combination of $L_P = (1 + 1/Q_0^2)$ and $G_P^{-1} = (1 + Q_0^2)R_{\text{loss}}$ where $Q_0 = L\omega_0/R_{\text{loss}}$ is the quality factor of the inductor at ω_0.

The nonlinear transfer characteristic of $-G_{\text{neg}}$ can be approximated by the following third degree polynomial. Even-order terms do not appear due to the nature of the fully differential circuit

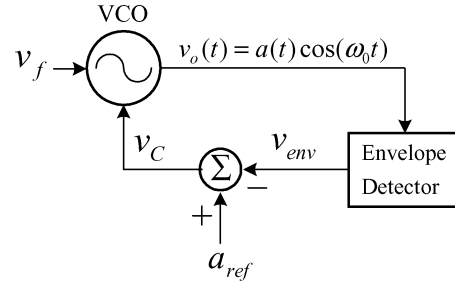$$i_{G_{\text{neg}}} = -a_1 v_{\text{out}} + a_3 v_{\text{out}}^3, \qquad a_1 > 0, a_3 > 0. \quad (1)$$

Applying Kirchoff's current law at the output node, the nonlinear differential equation governing the oscillator of Fig. 2 can be found as

$$\frac{d^2 v_{\text{out}}}{dt^2} - \frac{a_1 - G_p}{C}\left(1 - \frac{3a_3}{a_1 - G_p}v_{\text{out}}^2\right)\frac{dv_{\text{out}}}{dt} + \omega_0^2 v_{\text{out}} = 0 \quad (2)$$

where $\omega_0 \approx 1/\sqrt{L_P C}$.

Observe that (2) represents the self-sustained nonlinear equation describing the Van der Pol oscillator [9]. Assuming a steady-state response for the output voltage $v_{\text{out}}(t) = A_s\sin(\omega_0 t + \varphi)$ in Fig. 2, the describing function (DF) of $-G_{\text{neg}}$, which is the *linear* transconductance gain relating the amplitudes of the fundamental frequency component of the output current to that of the input voltage [10], can be expressed as $G_{\text{neg},DF} = (I_{G_{\text{neg}}}(s)/V_{\text{out}}(s)) = -a_1 + (3/4)a_3 A_s^2$. Thus, in the s-domain, the describing equation of the circuit can be expressed as

$$s^2 + b(A_s)s + \omega_0^2 = 0 \quad (3)$$

where $b(A_s) = (1/C)(G_p - a_1 + (3a_3/4)A_s^2)$.

In the oscillator's dynamic amplitude control mechanism, the position of the real part of the poles ($b(A_s)$ in (3)) depends on the oscillation amplitude A. If A is less than the desired steady-state amplitude A_s, the poles move into the right half plane, making the amplitude increase. If A is greater than A_s, the poles move into the left half plane, decreasing the amplitude. As a consequence of this property, the poles will stay on the imaginary axis for $A = A_s$. In other words, the stability condition [13] requires $(db(A_s)/dA) > 0$.

Next, VCO amplitude regulation techniques based on the LCF scheme currently available in the literature are discussed and the proposed scheme is presented afterwards.

B. Principles of the LCF Loop Technique

Fig. 3 shows the block diagram of an oscillator with a dynamic amplitude control mechanism in which v_f and v_C control the frequency and amplitude of the oscillation, respectively. In practical realizations of an oscillator, usually the signal v_C in Fig. 3 changes with ω_0, which means the oscillation amplitude changes as ω_0 changes even when the a_{ref} is fixed. As shown in Fig. 4(a), integrating the error signal v_C before going to the oscillator can minimize this effect [11]. Assuming v_C linearly controls the real part of the poles in (3) i.e., $B(s) = \alpha V_C(s)$,
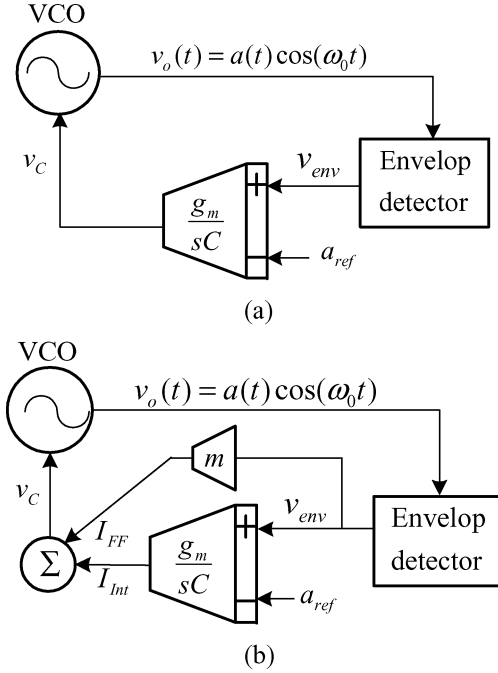
Fig. 4. Oscillator with amplitude regulation loop (a) unconditionally unstable automatic gain control (AGC) [11] (b) conditionally stable AGC using a feed-forward path [13].

the frequency response of the amplitude control loop in Fig. 4(a) [12] can be described as

$$A(s) = \frac{\frac{\alpha A_s}{2\tau_{\text{Int}}} A_{\text{ref}}(s)}{s^2 - \frac{\alpha A_s \tau_{\text{ENV}}}{2\tau_{\text{Int}}} s + \frac{\alpha A_s}{2\tau_{\text{Int}}}} \qquad (4)$$

where A_s, τ_{Int}, and τ_{ENV} are the oscillation amplitude at ω_0, the integrator, and the envelop detector time constants, respectively.

By observing the change of signs of the coefficients of the denominator of (4), based on the Routh–Hurwitz criteria, one can conclude the poles are located in the right half plane. This equation will be derived as a particular case of our proposed architecture in Section IV.

The loop in Fig. 4(a) can be made conditionally stable by introducing a feedforward path (m) as depicted in Fig. 4(b) and reported in [13]. Unfortunately, this scheme requires stringent limitations on m for stability purposes and degrades the phase noise of the oscillator by injecting the low frequency noise associated with the feedback loop to the control voltage v_C. This effect has been analyzed extensively in a bipolar implementation of the amplitude control loop in [14]. Next, an alternative solution is proposed which overcomes the previous drawbacks.

III. PROPOSED LCF LOOP

It can be shown that the transfer function of $V_C(s)/A(s)$ in the VCO of Fig. 4(a) has a $1/s$ characteristic (see (A5) and (A6) in the Appendix). Thus, the loop gain of the amplitude control loop in Fig. 4(a) has two poles at zero which makes the loop unstable. Thus, to improve the stability the pole associated with the integrator can be placed in a nonzero frequency which suggests the use of a lossy integrator in the loop.

Fig. 5 shows the proposed LCF loop scheme. This technique not only relaxes the stability requirement imposed on the local
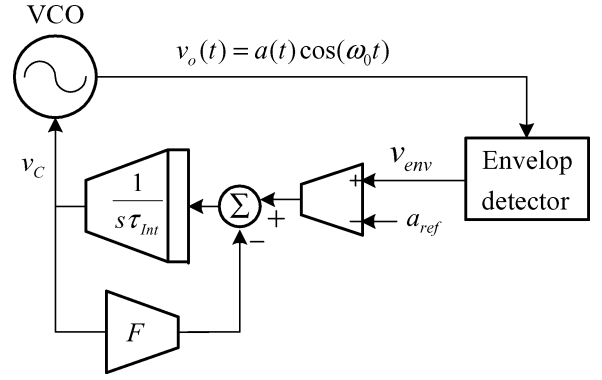
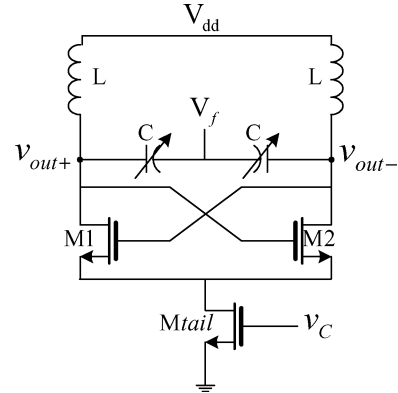

Fig. 5. Proposed LCF loop for amplitude tuning.

Fig. 6. *LC* oscillator (VCO) core in Fig. 5.

feedback F, to be discussed next, but it also generates a low pass filter which reduces and bounds the low frequency noise effect of the LCF loop. The frequency response of the amplitude control loop in Fig. 5 can be expressed as (see Appendix)

$$\begin{aligned} A(s) &= \frac{\frac{\alpha A_s}{2\tau_{\text{Int}}} A_{\text{REF}}(s)}{s^2 + \frac{1}{\tau_{\text{Int}}}\left(F - \frac{\alpha A_s \tau_{\text{ENV}}}{2}\right) s + \frac{\alpha A_s}{2\tau_{\text{Int}}}} \\ &= \frac{\omega_n^2 A_{\text{ref}}(s)}{s^2 + 2\xi\omega_n s + \omega_n^2}. \end{aligned} \qquad (5)$$

To guarantee the stability of (5), the coefficients of the denominator should have the same polarity, thus the following requirement for F can be obtained to ensure stability of the proposed LCF loop in Fig. 5:

$$F > \frac{\alpha A_s \tau_{\text{ENV}}}{2}. \qquad (6)$$

Equation (5) represents a second-order system with a damping factor of $\xi = (F - (\alpha A_s \tau_{\text{ENV}}/2))/\sqrt{2\alpha A_s \tau_{\text{Int}}}$ which for a critically damped step response, i.e., $\xi = 1/\sqrt{2}$, the exact value of F can be found as

$$F = \frac{\alpha A_s \tau_{\text{ENV}}}{2} + \sqrt{\alpha A_s \tau_{\text{Int}}}. \qquad (7)$$

In the case of the *LC* oscillator shown in Fig. 6, which is modeled in Fig. 2, the parameter α in the above expressions can be derived using the characteristic equation of the circuit

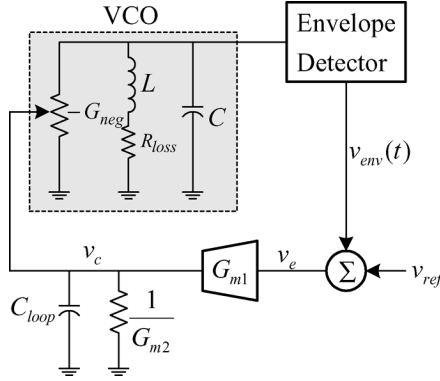$$s^2 + \frac{G_P - G_{\text{neg}}}{C} s + \frac{1}{L_P C} = 0. \qquad (8)$$

Fig. 7. Macromodel of the proposed LCF of Fig. 5.

Comparing (8) with (3) reveals that $b = (G_P - G_{\text{neg}})/C$ which for $G_{\text{neg}} = (1/2)\sqrt{\mu_n C_{\text{ox}}(W/L)_1 I_{\text{tail}}}$ and $I_{\text{tail}} = (1/2)\mu_n C_{\text{ox}}(W/L)_{\text{tail}}(V_C - V_{th})^2$ yields the following expression for α (see (A6)):

$$\alpha \approx \frac{\mu_n C_{\text{ox}}}{2\sqrt{2}C}\sqrt{\left(\frac{W}{L}\right)_1 \left(\frac{W}{L}\right)_{\text{tail}}} \tag{9}$$

where $(W/L)_1$ and $(W/L)_{\text{tail}}$ are the W/L ratios of M1 and Mtail in Fig. 6, respectively.

For typical values of $\alpha = 2 \times 10^9$, $A_s = 0.1$ V and $\tau_{\text{ENV}} = 2$ ns, (6) results in $F > 0.2$. Observe from (A8) that a higher value of F yields a higher damping factor ξ and thus less overshoot in the step response of the loop. However, a tradeoff should be considered, since in terms of circuit implementation, F represents the ratio of two different transconductance's and a higher F results in increased power consumption.

A. Transient Response of the Proposed LCF Loop

The effect of F on the transient response of the amplitude control loop in Fig. 6 can be explored using the model depicted in Fig. 7. The envelope detector in Fig. 7 is considered ideal. The parameter F in this model is equal to the ratio of G_{m2}/G_{m1}. A step input is assumed for the reference signal $a_{\text{ref}}(t)$ so that it changes from A_{r0} to A_{r1} at $t = 0$, and the corresponding steady-state oscillation amplitudes are A_{01} and A_{02}, respectively.

The control voltage v_c in Fig. 8 can be expressed as

$$v_c = \frac{G_{m1}}{G_{m2}}v_e - \frac{C_{\text{loop}}}{G_{m2}}\frac{dv_C}{dt} \tag{10}$$

where $v_e = a(t) - A_{02}$.

From (A3), it can be found that

$$\frac{da(t)}{dt} = -\frac{b(t)}{2}a(t). \tag{11}$$

By substituting (10) and (11) in (A6), the equation governing the transient behavior of the amplitude dynamics of the system in Fig. 7 can be solved

$$\frac{d}{dt}\left(\frac{\dot{a}}{a}\right) + \frac{1}{\tau_{\text{Int}}}\left(\frac{\dot{a}}{a}\right) + \frac{\alpha G_{m1}}{2C_{\text{loop}}}(a(t) - A_{02}) = 0 \tag{12}$$

where $\dot{a} = da(t)/dt$ and $\tau_{\text{Int}} = C_{\text{loop}}/G_{m2} = C_{\text{loop}}/(FG_{m1})$.

The numerical solutions of (12) for $A_{02} = 0.1$ V and for both the proposed (see (A8) and Fig. 5) and the reported amplitude control loops in Fig. 4 are shown in Fig. 8. As Fig. 8(a) shows, removing the local feedback F, which corresponds to $\tau_{\text{Int}} = \infty$, results in an unstable system [see Fig. 4(a)]. By using (A4) and following the above procedure used to derive (12), the poles of the unstable system are determined to be located at $\pm j\sqrt{\alpha G_{m1} A_s/(2C_{\text{loop}})}$.

In a similar way, the step response of the amplitude control loop in Fig. 4(b) is shown in Fig. 8(b). By selecting proper value of the feedforward m in this scheme, the loop can be stable. However, there is a large settling time at the output, which shows the behavior of a damped oscillation in the form of $e^{-\xi t}\sin\omega_f t$. In the previous expression for the output $\xi = 1/(2L(G_P - G_{\text{neg}}))$ and $\omega_f = \sqrt{\omega_0^2 - \xi^2}$ are the damping factor and the natural frequency of free oscillations in the circuit of Fig. 2.

In Fig. 7, when the local feedback $F = C_{\text{loop}}/(G_{m1}\tau_{\text{Int}})$ is present, the system becomes stable primarily due to a nonzero τ_{Int}. Depending on the value of τ_{Int}, the step response of the system can change from being over damped (small τ_{Int}) to under damped (large τ_{Int}). Assuming $G_{m1} = 1$ m/Ω, the transient response of (10) for three different values of F has been shown in Fig. 8(c). Note for a higher F, which corresponds with higher G_{m2}, results in a smaller τ_{Int} and thus smaller settling time. While increasing G_{m2} improves the settling time of the transient response, it also increases power consumption. The power consumed by G_{m2} can be expressed as

$$P_{\text{diss}} = V_{dd}I_{G_{m2}} = \frac{V_{dd}}{2\mu C_{\text{ox}}\left(\frac{W}{L}\right)_2}G_{m2}^2. \tag{13}$$

An optimum value of G_{m2} requires a trade off between the settling time of the step response of the amplitude control loop depicted in Fig. 8(c), and the power consumption described in (13). These two parameters, for $C_{\text{loop}} = 2$ pF and $(W/L)_2 = 50$, as a function of G_{m2} are plotted in Fig. 9.

B. Circuit Implementation of the Proposed LCF Loop

Fig. 10 shows the fully integrated circuit implementation of the proposed LCF loop together with the *LC* oscillator. Cross-coupled transistors M3-M4 compose the negative transconductance $-G_{\text{neg}}$ which is controlled by the tail current source (M5). The implemented inductors use the top metal layer and are designed and optimized using AISTIC [16]. The varactors are accumulation-mode pMOS capacitors, and are realized using multiple simple pMOS transistors connected in parallel with drain and source connected to ground. The control voltage v_f at the bulk terminal modifies the capacitance value of each varactor.

Fig. 11 depicts the circuit used as the envelop detector [17]. The main issue associated with the envelop detector is the tradeoff between its speed and accuracy. Increasing its bias current results in a faster transient response, while decreasing it improves the accuracy of the output voltage. The total parasitic capacitance at the output node is represented by C_{ENV}.

G_{m1} and G_{m2} cells used in Fig. 10 are implemented based on the simple three-current mirrors OTA's [15], and their ratio is determined by the stability factor $F = G_{m2}/G_{m1}$. A total capacitance of 2 pF is used to implement C_{loop}.
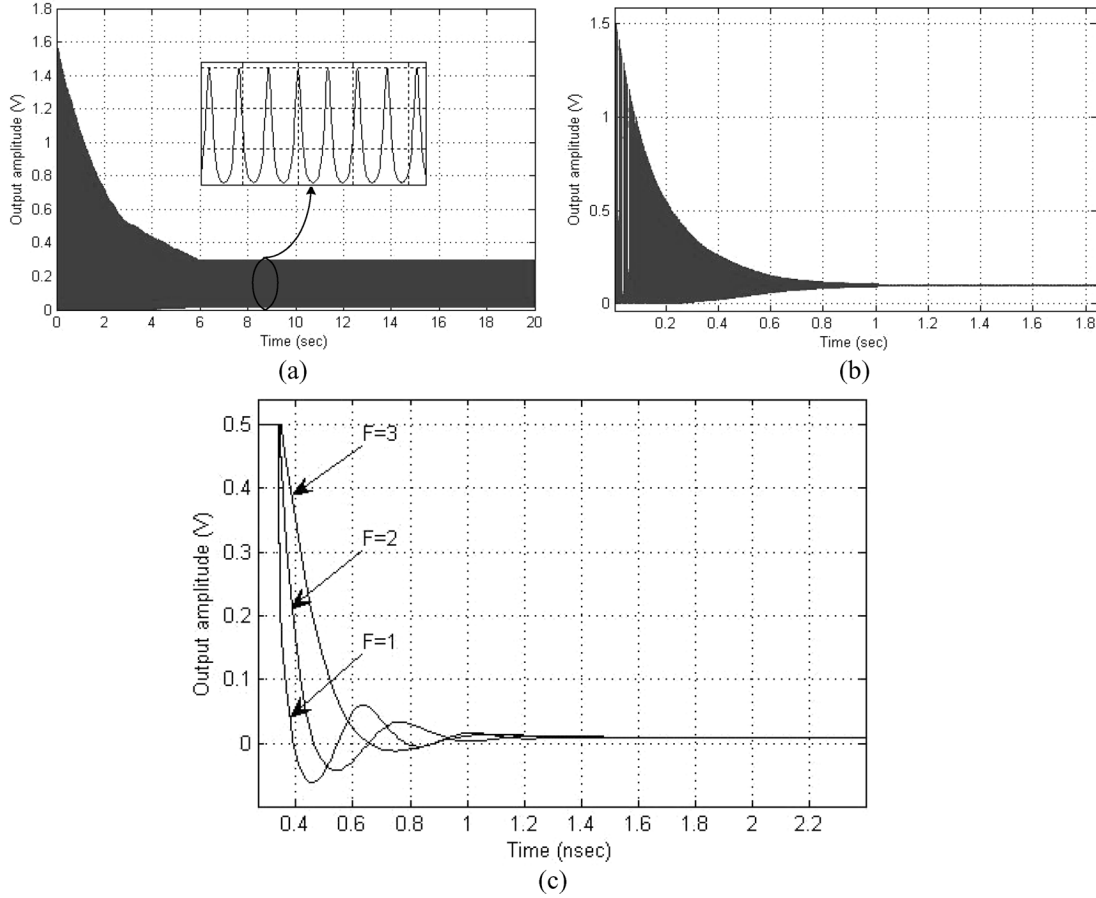
Fig. 8. Basic amplitude response of the (a) conventional control loop in Fig. 4(a), of the (b) control loop in Fig. 4(b), and of the (c) proposed control loop of Fig. 5.
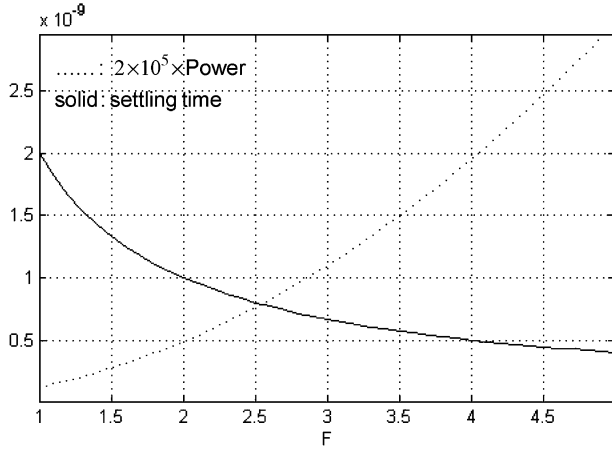

Fig. 9. Power consumption of G_{m2} cell and settling time as a function of F.

Fig. 10. Fully differential implementation of the proposed LCF loop.

IV. TEST CHIP MEASUREMENT RESULTS

A test chip has been fabricated in the TSMC 0.35-μm CMOS process available through, and thanks to, MOSIS. The chip micro photograph is shown in Fig. 12. The entire oscillator and the control loop, along with additional on-chip buffers, occupy an area of 0.038 mm^2 and 0.008 mm^2, respectively. All the measurements described in this section include the effect of the on-chip buffers with a measured attenuation of −20 dB at 2.2 GHz (for 50-Ω termination). The oscillator operates from a single 2.8-V supply voltage, and consumes 8-mA current. The oscillator operates from a minimum power supply voltage of 1.8 up to 2.8 V.
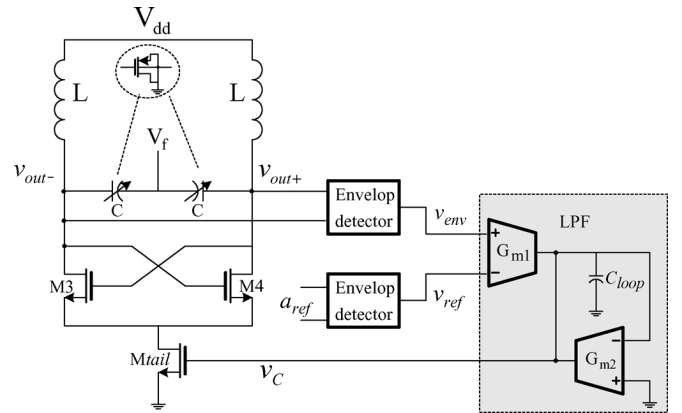
Fig. 13 shows the measured phase noise for an oscillation frequency of 2.3 GHz under the stable condition of $F = 2$. The phase noise at an offset frequency of 1 MHz from the carrier is −125 dBc/Hz. Note the feedback factor F in Fig. 5 can be changed using G_{m2} in Fig. 10. Reducing F to a value smaller than the critical value in (8) makes the LCF unstable. To verify this statement, Fig. 14 shows the measured phase noise of the unstable LCF loop, i.e., $F = 0$. Due to the instability of the loop, the control voltage v_C is changing and it modulates the amplitude and frequency of oscillation which results in the deterioration of the phase noise performance.
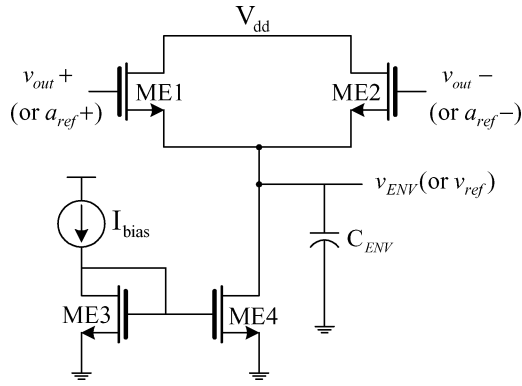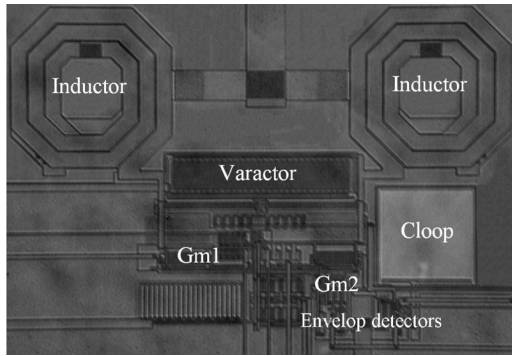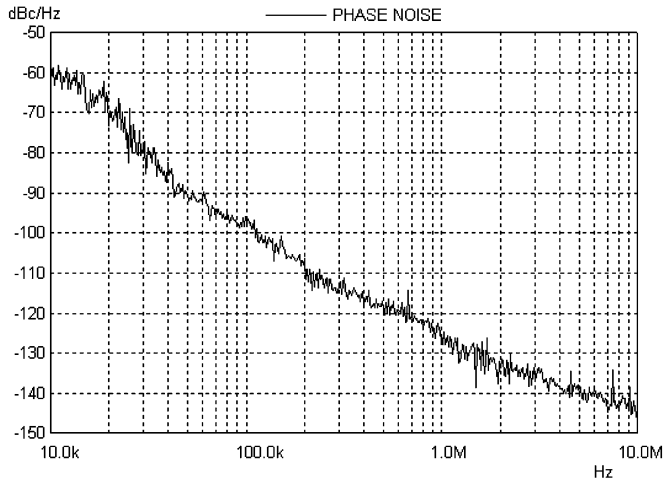
Fig. 11. Schematic of the envelop detector.

Fig. 12. Chip microphotograph.

Fig. 13. Measured phase noise of the VCO at 2.3 GHz under stable LCF loop condition, i.e., $F = 2$.

Fig. 14. Measured phase noise of the VCO at 2.3 GHz under unstable LCF loop condition, i.e., $F = 0$.

Fig. 15. Measured ac transient response of the feedback loop for $F = 2$ (dc level= 1.8 V and A_{ref} is a pulse wave with frequency of 20 MHz).

Fig. 16. Oscillation frequencies versus varactor control voltage as a function of the power supply.

The robust and stable step response of the proposed scheme is verified through measurement and this result is shown in Fig. 15. This figure shows the transient behavior of the control voltage v_C for a reference amplitude step from 2.8 to 2.2 V. The result shows a very close match with the behavioral model depicted in Fig. 8(c).

Fig. 16 shows the measured oscillation frequency range versus the tuning voltage vf as a function of the power supply. The results show the frequency range is fairly independent of the supply voltage and can vary from 2 to 2.5 GHz.
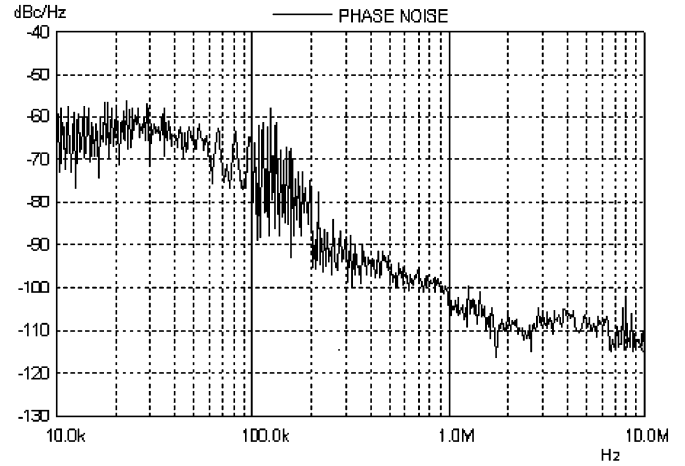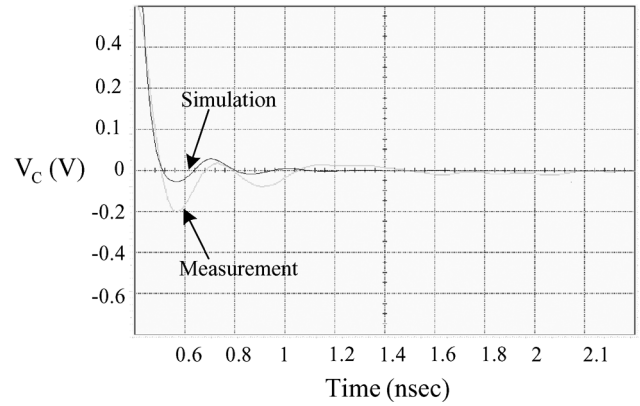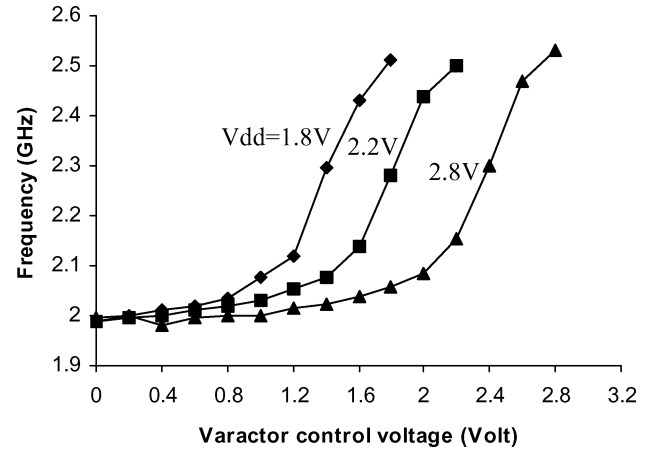
The oscillation amplitudes for four different reference voltages are measured and the results are shown in Fig. 17. By applying different reference amplitudes the control voltage v_C in Fig. 10 changes. Under this condition, the variation of the oscillation amplitude versus v_C is plotted in Fig. 18. The output amplitude shows a monotonic behavior with respect to the bias voltage of the tail current [6]. Fig. 18 also shows the HD3 of the output amplitude, as well as the measured phase noise at 1-MHz
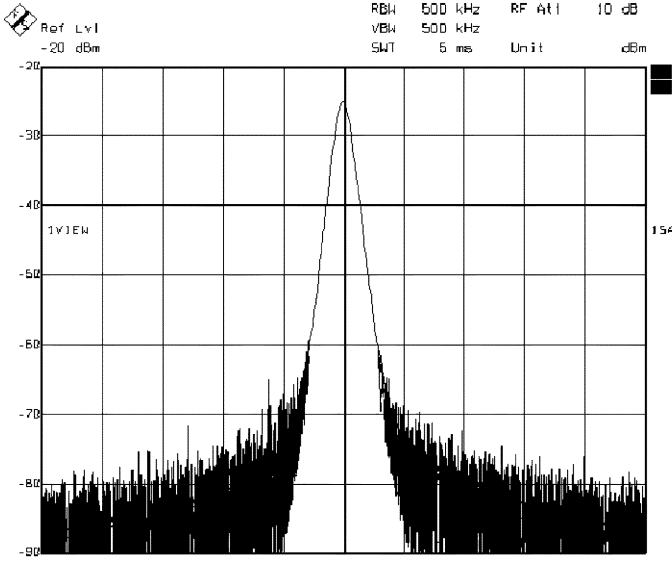
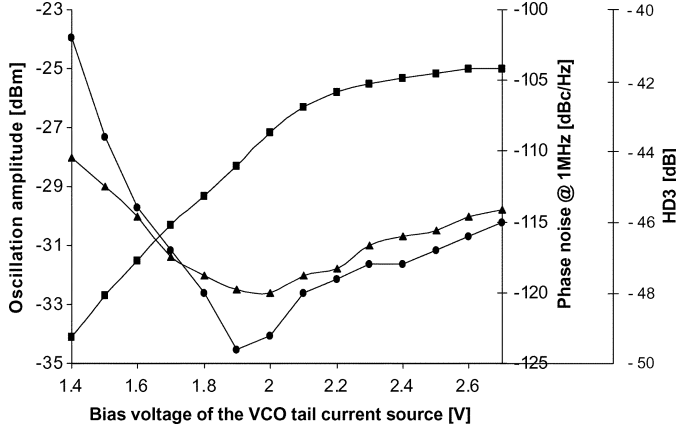Fig. 17. Measured oscillation amplitude for reference voltage of 2.5 V.

Fig. 18. Measured oscillation amplitude (■), phase noise (●) and HD3 (▲) versus the control voltage of the tail current source (v_C in Fig. 7).

TABLE I
VCO PERFORMANCE SUMMARY

Supply voltage (V)	2.8
Power consumption (mW): Core/LCF loop	22.4/0.3
Area (mm^2): Core/LCF loop	0.046/0.011
Center frequency (GHz)	2.3
Tuning range (GHz)	2 to 2.5
Phase noise (dBc/Hz) (f=2.3GHz, @1MHz)	-125

easy practical stability requirement. This requirement can be optimized to maintain a proper transient response with acceptable power consumption. The root of instability problems in controlling the amplitude of *LC* VCOs through LCF in previous publications is shown. Comparisons of the transient tests to the numerical solutions of the nonlinear equations describing the proposed feedback system have verified its theoretical characterization. Measurement results of the TSMC 0.35-μm CMOS implementation show an expected transient response for fast switching of the reference amplitude. The LCF loop, with respect to the VCO, has overheads of 1.3% and 24% on the area and power consumption, respectively.

APPENDIX
TRANSFER FUNCTION OF THE PROPOSED LCF LOOP

With regard to the selective properties of the resonant circuit of the oscillator, i.e., the first-order harmonic component markedly predominates over the other harmonics, we assume the solution in the form $\nu_{\mathrm{out}}(t) = a(t)\sin(\omega t + \varphi)$, where $a(t)$ is the waveform of the envelope with the steady-state amplitude of $a(\infty) = A_s$. Substituting $\nu_{\mathrm{out}}(t)$ in (2) and leaving out all the components other than the fundamental frequency, yields the following coefficients for sine and cosine terms, which must be identically zero

$$\left(\frac{G_P - a_1}{C} + \frac{3a_3}{4C}a(t)^2\right)\frac{da(t)}{dt}$$
$$+ \left(\omega_0^2 - \omega^2\right)a(t) = 0 \qquad (A1)$$
$$2\frac{da(t)}{dt} + \left(\frac{G_P - a_1}{C} + \frac{3a_3}{C}a(t)^2\right)a(t) = 0. \qquad (A2)$$

The steady-state oscillation amplitude A_s can be obtained from (A2) by setting $da(t)/dt = 0$. Thus, it can be shown that $A_s = 2\sqrt{a_1 - G_P/3a_3}$. However, the transient behavior of $a(t)$ before reaching the steady state can be analyzed by solving (A2) for $a(t)$

$$a(t) = a(t_0)\exp\left(-\frac{1}{2}\int_{t_0}^{t} b(\tau)d\tau\right)$$
$$= a(t_0)\left(1 - \frac{1}{2}\int_{t_0}^{t} b(\tau)d\tau + \frac{1}{8}\left(\int_{t_0}^{t} b(\tau)d\tau\right)^2 + \cdots\right) \quad (A3)$$

where $b(\tau) = (G_P - a_1/C) + (3a_3/C)a(\tau)^2$.

offset from the carrier frequency, as a function of the control voltage v_C. At lower control voltages, the oscillation amplitude is lower and the phase noise is relatively poor, but the HD3 is higher primarily due to the smaller voltage swing across the *LC* tank. At very high values of the control voltage, the tail current transistor (Mtail) moves to the triode region and this leads to larger noise sources in the tank. The increased noise in the tank degrades both phase noise and the HD3. The optimum point in this figure, in terms of the lowest phase noise value, occurs at a bias voltage around 2 V. At this bias, the variation of the oscillation frequency with respect to the tail current fluctuations is minimum. Table I summarizes the measured peformance of the amplitude controlled VCO under stable LCF loop condition ($F = 2$).

V. CONCLUSION

An LCF loop architecture capable of regulating the oscillation amplitude of *LC* resonators has been presented. The proposed architecture yields a simple, but stable LCF loop with an

For oscillation amplitude close to the stable amplitude $a(t_0) = A_s$, the term $b(t)$ in (A3) approaches zero and thus, the corresponding exponential term in (A3) can be approximated by its first-order Taylor expansion

$$a(t) \approx A_s - \frac{A_s}{2} \int_{t_0}^{t} b(\tau) d\tau. \tag{A4}$$

Note that $b(t)$ is a function of $a(t)$ and ω_0, and since $a(t)$ is controlled by v_C (see Fig. 5), in the frequency domain $B(s)$ is a function of s and $V_C(s)$. Therefore, in the frequency domain, (A4) can be expressed as

$$A(s) = -\frac{A_s}{2s} B(s, V_C). \tag{A5}$$

The dependence of B on V_C in (A5) depends on the implementation of the oscillator, but for small-signal analysis we may assume they are linearly dependent [13].

$$B(s) = \alpha V_C(s). \tag{A6}$$

To investigate the small-signal behavior of the LCF loop in Fig. 5, the envelope detector's output, $v_{\text{ENV}}(t)$, is assumed to always be a delayed version of $a(t)$. The justification of this assumption will be presented momentarily. Thus, the output of the envelope detector in frequency domain can be expressed as

$$V_{\text{ENV}}(s) = \frac{A(s)}{1 + s\tau_{\text{ENV}}} \cong A(s)(1 - s\tau_{\text{ENV}}) \tag{A7}$$

where τ_{ENV} is the time constant of the envelope detector.

Note that in the amplitude control loop in Fig. 5, $V_C(s)$ can be expressed as $(A(s)(1 - s\tau_{\text{ENV}}) - A_{\text{ref}}/F + s\tau_{\text{Int}})$. Thus, using (A5) and (A6), the frequency response of the LCF loop can be found as

$$A(s) = \frac{\frac{\alpha A_s}{2\tau_{\text{Int}}} A_{\text{REF}}(s)}{s^2 + \frac{1}{\tau_{\text{Int}}} \left(F - \frac{\alpha A_s \tau_{\text{ENV}}}{2} \right) s + \frac{\alpha A_s}{2\tau_{\text{Int}}}}$$

$$= \frac{\omega_n^2 A_{\text{ref}}(s)}{s^2 + 2\xi\omega_n s + \omega_n^2} \tag{A8}$$

where τ_{Int} is the time constant of the integrator in Fig. 5.

Based on the results obtained in Section III-B, the assumption used to derive (A7) can be justified. Assuming a critically damped response, using (7) and (A8), the closed-loop poles of the loss-control feedback in Fig. 5 can be expressed as

$$P_{\text{CL},1,2} = -\frac{1+j}{2} \sqrt{\frac{\alpha A_s}{\tau_{\text{Int}}}} \tag{A9}$$

To ensure that the envelope detector is faster than the closed-loop feedback, the frequency of amplitude variation, up to the closed-loop poles, should be smaller than the pole associated

with the envelope detector, i.e., $P_{\text{CL}1,2} < P_{\text{ENV}}$, in which $P_{\text{ENV}} = 1/\tau_{\text{ENV}}$. The subsequent result of this inequality is

$$\frac{\alpha \tau_{\text{ENV}}^2}{\tau_{\text{Int}}} < \frac{2}{A_s}. \tag{A10}$$

In practical implementations of the integrator and the envelope detector, and for typical values of C_{Int} (few picofarads) and C_{ENV} (hundreds of nanofarads), the inequality (A10) is easily satisfied.

REFERENCES

[1] W. Egan, "Modeling phase noise in frequency dividers," *IEEE Trans. Ultrason., Ferroelect., Freq. Contr.*, vol. 37, no. 3, pp. 307–315, Jul. 1990.

[2] S. Levantino, C. Samori, A. Bonfanti, S. L. J. Gierkink, A. L. Lacaita, and V. Boccuzzi, "Frequency dependence on bias current in 5-GHz CMOS VCOs: Impact on tuning range and flicker noise upconversion," *IEEE J. Solid-State Circuits*, vol. 37, no. 8, pp. 1003–1011, Aug. 2002.

[3] A. D. Berny, A. M. Niknejad, and R. G. Meyer, "A 1.8-GHz *LC* VCO with 1.3-GHz tuning range and digital amplitude calibration," *IEEE J. Solid-State Circuits*, vol. 40, no. 4, pp. 909–917, Apr. 2005.

[4] J. W. M. Rogers, D. Rahn, and C. Plett, "A study of digital and analog automatic-amplitude control circuitry for voltage-controlled oscillators," *IEEE J. Solid-State Circuits*, vol. 38, no. 2, pp. 352–356, Feb. 2003.

[5] R. Duncan, K. W. Martin, and A. S. Sedra, "A *Q*-enhanced active-RLC bandpass filter," *IEEE Trans. Circuits Syst. II, Analog Digit. Signal Process.*, vol. 44, no. 5, pp. 341–346, May 1997.

[6] A. Zanchi, C. Samori, S. Levantino, and A. L. Lacaita, "A 2-V 2.5-GHz–104-dBc/Hz at 100 kHz fully integrated VCO with wideband low-noise automatic amplitude control loop," *IEEE J. Solid-State Circuits*, vol. 36, no. 4, pp. 611–619, Apr. 2001.

[7] V. Aparin and P. Katzin, "Active GaAs MMIC bandpass filters with automatic frequency tuning and insertion loss control," *IEEE, J. Solid-State Circuits*, vol. 30, no. 10, pp. 1068–1073, Oct. 1995.

[8] F. Dülger, E. Sánchez-Sinencio, and J. Silva-Martinez, "A 1.3-V 5 mw fully integrated tunable bandpass filter at 2.1 GHz in 0.35-um CMOS," *IEEE J. Solid-State Circuits*, vol. 38, no. 6, pp. 918–928, Jun. 2003.

[9] F. Kouril and K. Vrba, *Non-Linear and Parametric Circuits*. London, U.K.: Wiley, 1988.

[10] A. Rodriguez-Vazquez, B. Linares-Barranco, J. L. Huertas, and E. Sánchez-Sinencio, "On the design of voltage-controlled sinusoidal oscillators using OTAs," *IEEE Trans. Circuits Syst. I, Fundam. Theory Appl.*, vol. 37, no. 2, pp. 198–211, Feb. 1990.

[11] E. Vannerson and K. C. Smith, "Fast amplitude stabilization of an *RC* oscillator," *IEEE J. Solid-State Circuits*, vol. 9, no. 4, pp. 176–179, Aug. 1974.

[12] D. Li and Y. P. Tsivids, "A loss-control feedback loop for VCO indirect tuning of RF integrated filters," *IEEE Trans. Circuits Syst. II, Analog Digit. Signal Process.*, vol. 47, no. 3, pp. 169–175, Mar. 2000.

[13] B. Linares-Barranco, T. Serrano-Gotarredona, J. Ramos-Martos, J. Ceballos-Caceres, J. M. Mora, and A. Linares-Barranco, "A precise 90 ° quadrature OTA-C oscillator tunable in the 50–130-MHz range," *IEEE Trans. Circuits Syst. I, Reg. Papers*, vol. 51, no. 4, pp. 649–663, Apr. 2004.

[14] A. Zanchi, C. Samori, A. L. Lacatia, and S. Levantino, "Impact of AAC design on phase noise performance of VCOs," *IEEE Trans. Circuits Syst. II, Analog Digit. Signal Process.*, vol. 48, no. 6, pp. 537–547, Jun. 2001.

[15] P. E. Allen and D. Holberg, *CMOS Analog Circuit Design*. New York: Oxford University Press, 2002.

[16] A. M. Niknejad and R. G. Meyer, "Analysis, design and optimization of spiral inductors and transformers for Si RF ICs," *IEEE J. Solid-State Circuits*, vol. 33, no. 10, pp. 1470–1481, Oct. 1998.

[17] J. Silva-Martinez, M. S. J. Steyaert, and W. Sansen, "Design techniques for high-performance full-CMOS OTA-RC continuous-time filters," *IEEE J. Solid-State Circuits*, vol. 27, no. 7, pp. 993–1001, Jul. 1992.

Faramarz Bahmani (S'01–M'03) received the B.Sc. degree from Tabriz University, Iran, the M.Sc. (Hons.) degree from Tehran University, Tehran, Iran, and the Ph.D. degree in electrical engineering from Texas A&M University, College Station, TX, in 1995, 1999, and 2006, respectively.

From 1999 to 2001, he was a Senior Design Engineer with Emad Semiconductors, Tehran, Iran, where he worked on high-speed analog circuit design. During the summer of 2005, he interned as a Circuit Design Engineer at Alvand Technology Inc., Santa Clara, CA, where he designed a wideband frequency synthesizer for video applications. He is currently with Scintera Networks Inc., San Jose, CA. His research interests include highly linear continuous-time filters, high-speed analog and mixed-signal circuits, and phase-locked loop based frequency synthesizers.

Edgar Sánchez-Sinencio (F'92) was born in Mexico City, Mexico. He received the degree in communications and electronic engineering (professional degree) from the National Polytechnic Institute of Mexico, Mexico City, Mexico, the M.S.E.E. degree from Stanford University, CA, and the Ph.D. degree from the University of Illinois at Champaign-Urbana, in 1966, 1970, and 1973, respectively.

He is currently the TI J Kilby Chair Professor and Director of the Analog and Mixed-Signal Center at Texas A&M University, College Station. He is coauthor of the book *Switched Capacitor Circuits* (Van Nostrand-Reinhold, 1984), and co-editor of the book *Low Voltage/Low-Power Integrated Circuits and Systems* (IEEE Press 1999). He has nearly 1000 citations reported in the Scientific Citation Index and has graduated more than 22 Ph.D. students and nearly 40 M.Sc. students. His present interests are in the area of RF-communication circuits and analog and mixed-mode circuit design.

Dr. Sánchez-Sinencio was awarded an Honoris Causa Doctorate by the National Institute for Astrophysics, Optics and Electronics, Mexico, the first honorary degree awarded for Microelectronic Circuit Design contributions, in November 1995. He is co-recipient of the 1995 Guillemin–Cauer award for his work on cellular networks. He is a former IEEE Circuits and Systems (CAS) Vice President-Publications. He was also the co-recipient of the 1997 Darlington Award for his work on high-frequency filters He received the IEEE CAS Society (CAS-S) Golden Jubilee Medal in 1999. He was the IEEE CAS-S Representative to the IEEE Solid-State Circuits Society (2000–2002). He was a member of the IEEE Solid-State Circuits Society Fellow Award Committee from 2002 to 2004. He is currently a member of the IEEE CAS-S Board of Governors. He was the General Chairman of the 1983 26th Midwest Symposium on Circuits and Systems. He was an Associate Editor for IEEE TRANSACTIONS ON CIRCUITS AND SYSTEMS (1985–1987) and an Associate Editor for the IEEE TRANSACTIONS ON NEURAL NETWORKS. He is the former Editor-in-Chief of the IEEE TRANSACTIONS ON CIRCUITS AND SYSTEMS—II: ANALOG AND DIGITAL SIGNAL PROCESSING.